

Design, implementation, and characterization of a kinematically aligned, cascaded spot-array generator for a modulator-based free-space optical interconnect

Daniel F.-Brosseau, Frédéric Lacroix, Michael H. Ayliffe, Eric Bernier, Brian Robertson, Frank A. P. Tooley, David V. Plant, and Andrew G. Kirk

The design and the implementation of a modular spot-array generator for a modulator-based free-space optical interconnect is presented. Two cascaded diffractive optical elements produce 4×8 clusters on a $1600 \mu\text{m} \times 800 \mu\text{m}$ pitch, where each cluster is a 4×4 array of $(1/e^2)$ $13.1\text{-}\mu\text{m}$ -radius spots on a $90\text{-}\mu\text{m}$ pitch. The spot-array generator is kinematically aligned to the interconnect system such that no realignment is necessary between removal and reinsertion. Characterization results are presented.

© 2000 Optical Society of America

OCIS codes: 200.2610, 200.4650, 050.0050.

1. Introduction

Two-dimensional (2-D) free-space optical interconnects represent a possible solution for alleviating some of the interconnection bottlenecks currently experienced by high-performance electronic systems.¹ The two most widely investigated optoelectronic technologies for free-space optical data transmission are arrays of multiple-quantum-well (MQW) modulators and of vertical-cavity surface-emitting lasers²⁻⁴ (VCSEL's). VCSEL's have many interesting optical characteristics,^{5,6} and significant progress in their development such as their integration with complementary metal-oxide semiconductor (CMOS) technology has recently been achieved.⁷ However, the design of compact optical interconnects that possess a large number of optical channels would require

large arrays ($>32 \times 32$) of single-mode VCSEL's demonstrating both good uniformity and stability that are hybridized to CMOS integrated circuits. At the time the research reported here was conducted such devices were not yet available. Furthermore, the threshold uniformity and the thermal management of large VCSEL arrays remains a challenge.

In contrast, large arrays of MQW modulator devices flip-chip bonded to CMOS's with excellent characteristics have already been demonstrated.⁸ This proven technology has been employed by many research groups for the realization of free-space optical interconnects.⁹⁻¹¹ Recently, a modulator-based free-space optical interconnect was developed for optical backplane applications.¹² The system uses a minichannel-based interconnection scheme¹³ in which a telecentric lenslet arrangement allows multiple signal beams to be relayed through each minichannel. A clustered-window geometry in which optoelectronic devices are physically grouped in a 4×4 matrix about the axis of each minichannel is employed. There are 8×8 minichannels of such 4×4 clusters, which results in a system with 1024 optical channels. Modulator-based systems require that the modulators be illuminated with a 2-D array of uniform cw readout beams. This requirement motivates the need to develop a suitable spot-array generator. In this paper the design and the implementation of an array generator for such a clustered optical interconnect is described.

When this study was performed, the authors were with the Photonic Systems Group, Department of Electrical and Computer Engineering, McGill University, 3480 University Street, Montréal, Québec H3A 2A7, Canada. B. Robertson is now with Thomas Swan and Company, Ltd., c/o Department of Engineering, Cambridge University, Cambridge CB2 1PZ, UK. F. A. P. Tooley is now with the Department of Physics, Heriot-Watt University, Edinburgh EH14 4AS, Scotland. D. F.-Brosseau's e-mail address is danielb@photonics.ece.mcgill.ca.

Received 24 May 1999; revised manuscript received 25 October 1999.

0003-6935/00/050733-13\$15.00/0

© 2000 Optical Society of America

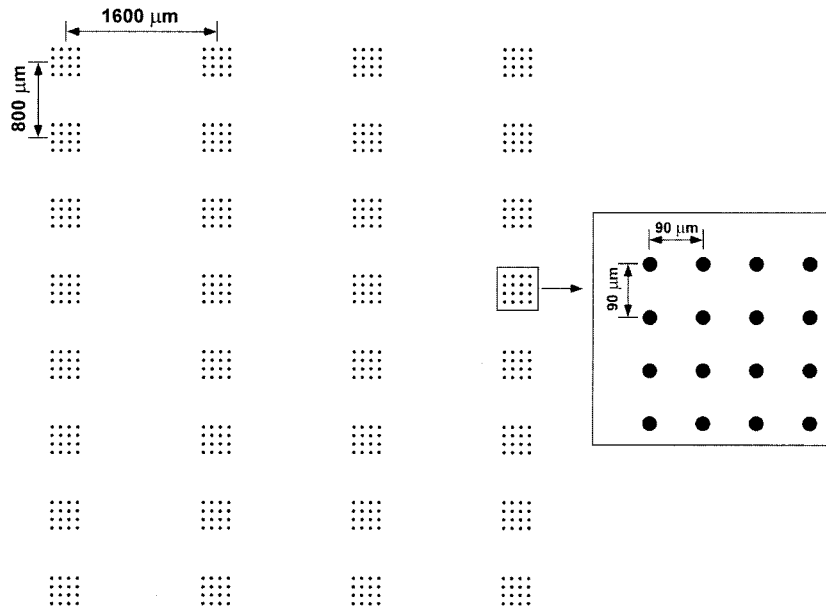


Fig. 1. Schematic diagram of the spot-array generator.

Although numerous techniques exist for generating spot arrays,¹⁴ most free-space optical interconnects rely on the Fourier plane array-generation technique.^{14–18} To read out the logical state of the modulators, it is necessary for the system described here to have an array of 4×8 clusters on a $1600 \mu\text{m} \times 800 \mu\text{m}$ pitch in which each cluster is an array of 4×4 spots on a $90\text{-}\mu\text{m}$ pitch (see Fig. 1). The geometry of the clustered spot array can easily be implemented by the cascading of two Fourier plane array generators. A cascaded implementation possesses the advantage of producing a spot array with higher uniformity than that produced by a single Fourier plane array generator.¹⁹

Spot-array generators have been implemented by use of different techniques and packaging approaches.^{9–11,20} However, not much emphasis has been placed on developing an array-generation system that is compact and modular and that can be aligned kinematically with the optical interconnect. It is advantageous for scalable multistage systems if optical array generators are designed as separate modules that are prealigned and then mounted on the system. Furthermore, it is important that such a module be easy to assemble. Finally, to facilitate test and repair, it is necessary that the module be designed such that it can be unmounted and remounted on the system without realignment. All these concerns have been addressed by the design of the spot-array generator for our proposed system.

The format of this paper is as follows: Section 2 presents a short overview of the optical interconnect system. The optical and the optomechanical requirements for the spot-array generator are introduced in Section 3. Section 4 presents the optical design of the cascaded array-generator system,

whereas the optomechanical design is presented in Section 5. The assembly and the alignment procedures of the optical-power-supply (OPS) module is discussed in Section 6. Section 7 describes the kinematic-alignment mechanism of the array generator to the optical interconnect. Finally, Section 8 presents characterization results.

2. Optical Interconnect Overview

The design of the optical interconnect was described in Ref. 12. This system, which interconnects optoelectronic VLSI (OE-VLSI) chips in a unidirectional ring (see Fig. 2), is designed to be scalable (to an arbitrary even number of boards), modular (to allow easy assembly and maintenance), compact, robust, and misalignment tolerant. The OE-VLSI chips are based on GaAs/AlGaAs MQW electroabsorption modulators and p-i-(MQW)-n detectors, which are

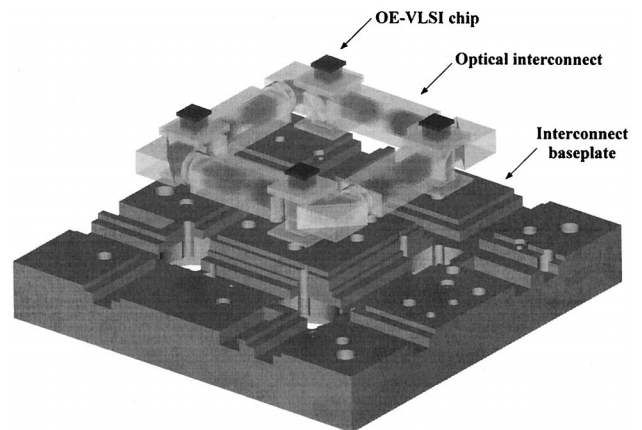


Fig. 2. Schematic diagram of a ring-based optical backplane that requires the proposed spot-array generator.

Table 1. OPS Requirements

Element	Requirement	Measured
Optical elements		
Wavelength	852.0 nm	852.0 ± 0.1 nm
4×8 Cluster array pitch	$1600 \mu\text{m} \times 800 \mu\text{m}$	$1602.2 \pm 0.4 \mu\text{m} \times 801.5 \pm 0.2 \mu\text{m}^a$
4×4 Cluster array pitch	$90 \mu\text{m} \times 90 \mu\text{m}$	$89.1 \pm 0.2 \mu\text{m} \times 89.1 \pm 0.2 \mu\text{m}$
Beam waist at the modulators ($1/e^2$)	13.1 μm	$\omega_x = 13.7 \pm 0.1 \mu\text{m}^a$ $\omega_y = 13.4 \pm 0.1 \mu\text{m}^a$
Input-polarization linearity	>100:1	1500:1
Optomechanical elements ^b		
Roll around the optical axis	45 arc min (0.75°)	<6 arc min (0.1°)
Lateral-alignment repeatability	55 μm	$\sigma_x = 5.8 \mu\text{m}$ $\sigma_y = 4.1 \mu\text{m}$
Angular-alignment repeatability	3 arc min (0.05°)	$\sigma_x = 0.004^\circ$ $\sigma_y = 0.006^\circ$

^aWorst case out of four implementations.

^bRequirements for a 1% loss in the optical power throughput through the interconnect.

the interconnect baseplate. The optical interconnect design requires that the optical axis of the OPS module be aligned at 90° to that of the interconnect system (as shown in Fig. 3). To allow for simple replacement and repair procedures, it is also desirable for a kinematic-mounting mechanism to be developed such that the OPS module can be unmounted and remounted without requiring any realignment. Finally, the optomechanical design should be compact, robust, and easy to assemble, while minimizing cost.

An analysis of the tolerances for the alignment of the OPS module to the interconnect optics was presented in Ref. 21. The requirements listed in the second section of Table 1 represent the alignment tolerances associated with a 1% loss in the optical power throughput through the interconnect. Because this metric is conservative, the system can still operate if these tolerance specifications are not met. However, a further increase in system misalignment will ultimately translate into lower operating speeds or larger bit-error rates.

4. Optical Design

A. Design Choices

Various possibilities were examined for the design of the array generator. The most obvious solution would be to generate the entire spot array with a single diffractive optical element and a Fourier lens. However, to produce the required array of 512 beams and achieve good uniformity would require a diffractive optical element of at least 2048×2048 pixels,²⁴ which would represent a significant design challenge. Another possibility would be to use an $8f$ optical system with two array-generation stages consisting of a 4×8 generator and a single 4×4 array generator with three identical Fourier lenses (as demonstrated in Ref. 16). However, this scheme represents a bulky system that does not scale well. Furthermore, because the beam divergence required at the modulator array is determined by the design of the inter-

connection system and because the minilenses that are used to route light through the system are already in place in front of the modulators, it was also desirable to use those lenses as part of the array-generation system. This decision led to the design described in Subsection 4.B.

B. Cascaded Array-Generation System Design

A schematic drawing of the array-generation system design is shown in Fig. 4. Two Fourier plane array generators are cascaded to produce the required array of 512 beams. The first stage produces an array of 4×8 beams on a $1600 \mu\text{m} \times 800 \mu\text{m}$ pitch, which corresponds to the layout of modulator clusters on the OE-VLSI chip. Each of these beams is then fanned out into an array of 4×4 spots on a $90\text{-}\mu\text{m}$ pitch. The Fourier plane array generators are computer-generated holograms implemented as a binary-level (4×8 fan-out) and a multiple-level (4×4 fan-out) phase grating.

There are four lens transformations in the array-generation system:

- (i) The collimation of the beam emitted from the fiber.
- (ii) The focusing of the collimated beam at the output of the Fourier lens.
- (iii) The collimation of the beam at the output of the OPS module.
- (iv) The focusing of the collimated beam onto the modulators.

With the Gaussian beam-propagation model it is possible to calculate the required beam waists in the array-generation system. Because of the telecentricity of the system, all waists are located at the focal points of the different lenses. Given a lens of focal length f with an input beam waist of ω_0 , the output beam waist ω_0' is approximately equal to

$$\omega_0' \approx \frac{\lambda}{\pi\omega_0} f, \quad (1)$$

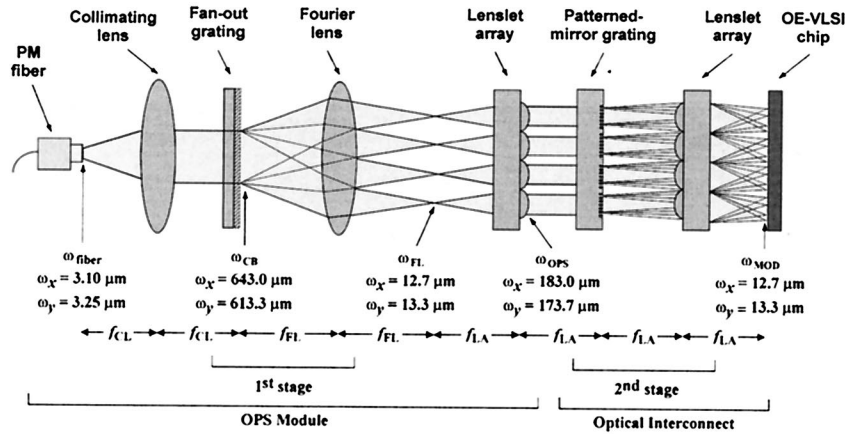


Fig. 4. Design of the array-generation system. (For simplicity polarization and beam-steering components are not shown.)

given that $2z_0 \gg f$ for all four lens transformations²⁵ (z_0 is the Rayleigh range). The calculated beam waists for all lens transformations are shown in Fig. 4. Note that, because the system is telecentric, the beam waist at the focus of the Fourier lens ω_{FL} is the same as that at the modulators ω_{MOD} . A polarization-maintaining (PM) fiber was used to deliver polarized light to the system. The mode-field diameter (or $2\omega_{fiber}$) of such a fiber is not perfectly circular; it was measured to be $6.5 \mu\text{m}$ in x and $6.2 \mu\text{m}$ in y . The effective focal length of the collimating lens that is required to produce a beam with the required waist ω_{CL} is $f_{CL} = 7.35 \text{ mm}$.

C. Optical-Power-Supply Module Optical Design

The OPS module implements the first stage of the array-generation system. Because the module is assembled and characterized separately, a separate set of requirements was developed for the output beams of the OPS module. It is necessary to produce an array of 4×8 collimated beams with a waist of $\omega_{OPS} = 176.0 \mu\text{m}$ on a $1600 \mu\text{m} \times 800 \mu\text{m}$ pitch. The optical design should provide a means of laterally translating the beams by $\pm 300 \mu\text{m}$ such that they can be aligned with the OE-VLSI chip after the OPS module is inserted into the interconnect baseplate. Finally, the state of polarization of the light must be right-hand circular for it to be routed properly in the

interconnect system. The objective for the OPS module optical design is to meet all these requirements while reducing the optomechanical complexity to a minimum. To do so, it is necessary that a number of optical and optomechanical degrees of freedom be incorporated in the design of the OPS module. These design items are presented in Table 2.

A schematic diagram of the OPS module's optical design is shown in Fig. 5. The light is delivered through a fiber-connect (FC) PM single-mode fiber. The light output from the PM fiber shows excellent polarization characteristics and has an extinction ratio greater than 1500:1. For design simplicity it was decided to use off-the-shelf lenses to collimate the light from the PM fiber. A combination of an aspheric lens ($f = 6.26 \text{ mm}$) and a negative achromatic lens ($f = -20.14 \text{ mm}$) was chosen to reduce aberrations. The spacing between the lenses is variable to accommodate for variations in the divergence of the light emitted by the fiber and for deviations of the focal length ($\pm 1\%$) such that the effective focal length can be adjusted to $f_{CL} = 7.35 \text{ mm}$. Because the light at the output of the fiber is linear and p polarized, a QWP is used to change the state of polarization to right-hand circular. The beam then passes through a 0.5° Risley prism pair (RPP) that provides a $\pm 330\text{-}\mu\text{m}$ lateral adjustment of the spot array.

The fan-out grating (FOG) is a Fourier plane array

Table 2. OPS Module Degrees of Freedom

Design Requirement	Optical-Optomechanical Solution
Spots on a uniform grid Spot pitch of $1600 \mu\text{m} \times 800 \mu\text{m}$	Low-distortion Fourier lens Adjust focal length of Fourier lens with a change in element separation
Spot size of $13.1 \mu\text{m}$ ($1/e^2$)	Adjust focal length of collimating lens with a change in element separation
Collimated beam through the fan-out grating (FOG) Angular alignment of the collimated beam Angular alignment of the spot array about the optical axis Mutual angular alignment of the chief rays of all beams in the spot array Lateral alignment of the spot array	Maintain the fiber facet at the front focus of the collimating lens Adjust the fiber-receptacle lateral position on the collimation barrel Rotate the FOG about the optical axis Position the FOG at the front focus of the (low-aberration) Fourier lens Rotate the RPP's about the optical axis

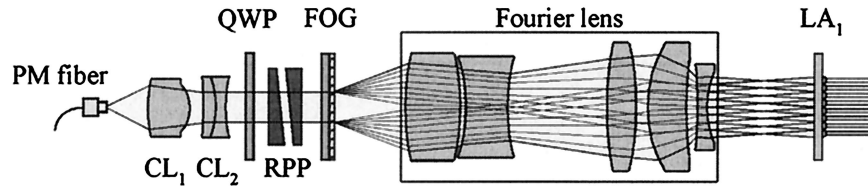


Fig. 5. Schematic diagram of the OPS module optical design. CL, collimating lens; LA, lenslet array.

generator that is placed at the waist of the collimated beam. This binary diffractive element has a period of $32\ \mu\text{m} \times 64\ \mu\text{m}$ and is designed to produce an array of 4×8 diffraction orders (odd orders only). The FOG can be rotated to align the spot array with respect to the optical axis.

The optical properties of the Fourier lens have an influence on numerous characteristics of the 4×8 spot array (see Table 2): The choice of the Fourier lens is thus an important one. A detailed description of the chosen Fourier lens can be found in Ref. 11. The lens comprises five elements and achieves good correction for the achromatizing aberrations, such as spherical, astigmatism, and distortion aberration. It also provides a large field size (7.7 mm), while maintaining low field curvature and distortion ($f - \sin \theta$ distortion of less than 0.025% across the 20.7° field of view). The design allows the Fourier lens's focal length to be adjusted precisely to $f_{\text{FL}} = 30.00$ mm by variation of the spacing of the last element, which acts as a field flattener. This adjustment is necessary because the required focal-length control for achieving a $1\text{-}\mu\text{m}$ spot-position error is 1 part in 2000 (Ref. 11). Finally, the optical elements are packaged in a magnetic stainless-steel barrel with an outer diameter of 25.00 mm.

The last element of the OPS module is an array of 8×8 minilenses on an $800\text{-}\mu\text{m}$ pitch ($f_{\text{LA}} = 8.5$ mm), and it is used to collimate the beams. The minilenses in this system all have the same design and are eight-level diffractive elements.

D. Second-Stage Optical Design

The second stage of the array-generation system (as shown in Fig. 4) consists of a FOG in combination with a lenslet array that acts as a Fourier lens. The patterned-mirror grating (PMG) consists of four FOG stripes interlaced with four metal-mirror stripes. The grating, which is an eight-level element, has a period of $161\ \mu\text{m}$ and is designed to produce a 4×4 array on a $90\text{-}\mu\text{m}$ pitch when used in combination with an 8.5-mm Fourier lens. The waists of the collimated beams produced by the OPS module must be incident upon the grating, and the lenslet array must be placed at a distance f_{LA} from the PMG for each beam to be divided into the required spot array. The PMG is assembled as part of the beam-combination module²¹ and packaged in the interconnect baseplate. The metal stripes are used in the interconnect to reflect data from the previous stage onto the receivers (see Fig. 3). Finally, the lenslet array is packaged as part of the chip module.²²

E. Design Modeling and Simulation

The optical design was modeled by use of commercial ray-tracing software. The point-spread function and the Strehl ratio were calculated for the spots at the modulators. The calculations were performed for two different spots: the center spot, which is located on the optical axis (i.e., the zero order for both the FOG and the PMG), and the outer spot, which is the farthest from the optical axis in the 512-spot array. The outer spot is located at a distance of $3878\ \mu\text{m}$ from the optical axis. Because the simulation software does not allow for array propagation, an equivalent optical system was designed by the modification of the period of the gratings such that a spot is produced on the y axis at the required distance from the optical axis.

The point-spread function indicates that the center and the outer spot radii ($1/e^2$) are $13.7\ \mu\text{m}$, which is slightly larger than the Gaussian beam design value ($13.1\ \mu\text{m}$). This minimal increase, which results in a spot of $3\omega = 41.1\ \mu\text{m}$, can be tolerated by the oversized modulators ($50\ \mu\text{m}$) and detectors ($70\ \mu\text{m}$). The Strehl ratios for the center and the outer spots are, respectively, 0.892 and 0.886. These ratios indicate that aberrations are reduced to the Rayleigh limit,²⁶ and the system can therefore be considered to be diffraction limited. Finally, Gaussian beam-propagation simulation confirmed the calculated beam waists presented in Fig. 4.

5. Optomechanical Design of the Optical-Power-Supply Module

For addressing the optomechanical requirements presented in Subsection 2.B different packaging strategies are available. For example, a barrel assembly was employed in a previous implementation of an OPS.²⁰ However, it was found that the barrel assembly is not ideal for implementation. First, the components are not easily accessible when housed in a barrel: Their insertion, removal, and repositioning are tedious and time consuming. Second, the mounting of the barrel assembly onto a baseplate lacks sufficient insertion accuracy.

The packaging strategy for the OPS module in this system consists of centering the optical components in 25.00-mm magnetic stainless-steel cells and then depositing them onto a baseplate. The baseplate is made of a rectangular slot with two precision-ground rods positioned in the corners of the slot, the rods acting as rails for the cells. Rare-earth magnets are glued onto the bottom of the slot; they constrain the

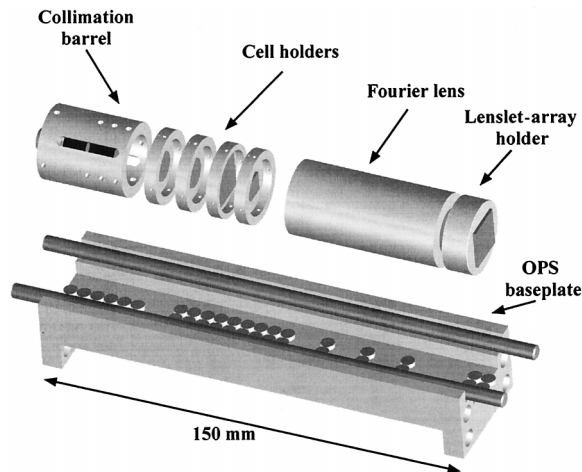


Fig. 6. Schematic diagram of the OPS module optomechanics.

cells laterally and angularly. This strategy is similar to those presented in Refs. 27 and 28 in which either a V groove or a rectangular slot was used to support the components and define two reference axes for their alignment. Of these two strategies the V groove provides the most effective alignment because the line of contact on the baseplate lies on a planar surface (as opposed to a sharp corner in the case of the rectangular slot). Indeed, the drawback to rectangular-slot baseplates is their poor alignment repeatability owing to the degradation of the edge's sharpness after repeated insertions. On the other hand, the drawback to V grooves is an increase in machining cost. The baseplate approach that is proposed here combines both of these advantages: alignment repeatability and ease of machining. Furthermore, a derivative and significant advantage for using rods as an alignment reference is that they can be used to align the OPS module kinematically to the interconnect baseplate because they define the optomechanical axis of the OPS module. The mounting technique of the OPS baseplate to the interconnect baseplate is described in Section 7.

A schematic diagram of the optomechanics is shown in Fig. 6, and the different optomechanical components are described in the following subsections. In the discussion, lateral alignment refers to the direction perpendicular to the optical axis of the OPS module (x - y), whereas longitudinal alignment refers to the direction of light propagation, that is, parallel to the optical axis of the OPS module (z).

A. Optical-Power-Supply Baseplate

The support for the cells of the OPS module consists of a slot baseplate 150 mm (long) \times 40 mm (wide) \times 15 mm (high) with the two extremities being 25 mm high. For ease of machining and reducing weight the OPS baseplates are machined out of aluminum. The baseplate is also compatible with ϕ 25-mm commercial optomechanical components so that the OPS modules can easily be assembled and characterized separately.

For accurately defining the distance between the rods and ensuring their parallelism two alignment holders are used to position and align the rods on the OPS baseplate. Each holder consists of a rectangular piece through which two holes providing a tight sliding-fit clearance for the rods have been machined. The holes on the holders are machined such that their position is within 5 μ m of the design value. Because the rods are aligned with the help of holders, the machining tolerances of the OPS baseplate, such as the position and the width of the slot, can be relaxed. Only one pair of holders is necessary to align the rods on all four OPS baseplates.

B. Cell Holders

All cells are machined out of 416 magnetic stainless steel such that they can be held in place by the magnets in the OPS baseplate during their alignment. The lateral alignment of the QWP, the RPP's, and the FOG is not critical. Thus the components are positioned manually and glued to 25-mm cells. On the other hand, the fiber, collimating lenses, Fourier lens, and lenslet array must be aligned accurately to a common optical axis. To do so requires that the components be centered within cells machined to an outer diameter of 25.00 ± 0.01 mm. The lenslet-array alignment technique utilizes lithographically defined metal markers that are deposited on the substrate during the lenslet-etching process. The lenslet array is centered relative to its cell by the alignment of the markers present on the substrate to those machined on the cell. It is then fixed by use of UV-cured epoxy; its alignment precision to the optomechanical axis of the cell was measured to be within 30 μ m.

C. Collimation Barrel

It was decided to mount the fiber and the collimating lenses in a single barrel, referred to as the collimation barrel (see Fig. 7). This approach allows the collimating module to be easily inserted and removed from the OPS module, while maintaining alignment and collimation accuracy. The aspheric and the achromatic lenses are first mounted in Delrin cells by use of an interference fit between the cell and the lens-edge surfaces.²⁹ This type of fitting automatically centers the lenses to the mechanical axes of their cells. The outer diameters of the Delrin cells are machined to provide a close sliding-fit clearance to the inner diameter of the collimation barrel so that they can easily be inserted and removed from the barrel, while ensuring their alignment with its optomechanical axis.

The interior of the collimation barrel is divided into two sections by a stopper: The fiber receptacle is placed on one side, whereas the collimating lenses are inserted on the other side. The longitudinal positions of the lenses are adjusted by a combination of spacers inserted between the stopper and the first collimating lens and between the two lenses. The spacers and the lenses are held in place with a retainer ring that is fixed by use of four screws. Fi-

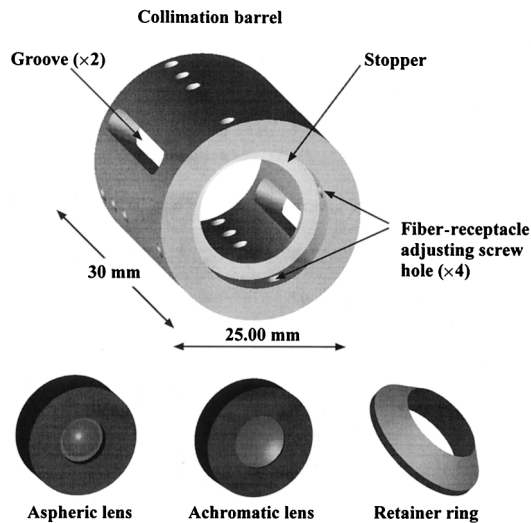


Fig. 7. Schematic diagrams of the collimation barrel and its components.

nally, the design of the collimation barrel includes a groove to allow easy access to the cells inside the barrel.

The mechanism for centering the fiber with the optomechanical axis of the collimation barrel is shown in Fig. 8. The end plate of a FC-physical-contact fiber receptacle is chamfered down at 45° , as shown. The fiber receptacle is placed in contact with the stopper of the collimation barrel and four cup-point-locking screws (to minimize backlash and provide stable positioning) are driven against the chamfered edge to hold the receptacle in place. The screws are then used to adjust the lateral position of the fiber receptacle. Using this mechanism allows the fiber to be centered to the optomechanical axis of the collimation barrel with a precision of better than $6 \mu\text{m}$. Furthermore, after numerous removals from and insertions into the receptacle of the fiber the deviation of the fiber from its initial position is within $1 \mu\text{m}$. This mechanism is an improved version of that presented in Ref. 20 in which the receptacle was

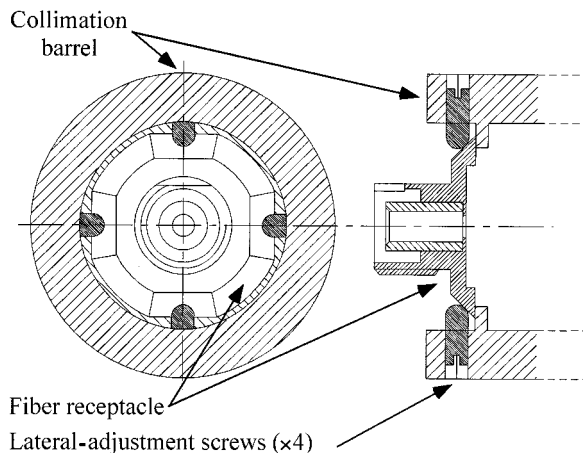


Fig. 8. Schematic diagram of the fiber-centering mechanism.

chamfered down in a circular fashion and permitted an alignment precision of $10 \mu\text{m}$.

6. Assembly and Alignment

The first step in the assembly of the OPS module is the assembly of the collimation barrel. After the receptacle has been centered the design requires that the positions of the collimating lenses be adjusted to produce a collimated beam with a waist radius between $610 \mu\text{m} < \omega_{\text{CB}} < 640 \mu\text{m}$ in both x and y . However, it was found that the size of the beam waists needed to be slightly larger than the theoretical value, that is, between $640 \mu\text{m} < \omega_{\text{CB}} < 670 \mu\text{m}$, to produce the required spot size ($13.1 \mu\text{m}$) at the modulators. This need can be explained by the tolerance on the focal length of different components in the OPS module and the optical interconnect and by possible variation of the mode-field diameters for different fibers.

It was noted that the beam at the output of the collimation barrel had a small angular deviation with respect to the optomechanical axis of the barrel. This deviation can be attributed to the sliding-fit clearance required for the insertion of the cells into the collimation barrel, resulting in the lenses being not perfectly centered on the optical axis. However, this angular deviation can be reduced to less than 0.01° by a slight adjustment of the position of the fiber receptacle to compensate for this misalignment.

The second step of the assembly consists of adjusting the focal length of the Fourier lens to produce a spot array with the required pitch. To do so requires that an alignment mask replicating the ideal spot position be designed and mounted on a cell by use of the same technique as for the lenslet array (Subsection 5.B). Positioning the collimation barrel, the FOG, the Fourier lens, and the alignment mask on the OPS baseplate allows the spot array to be observed on the alignment mask. The focal length of the Fourier lens is then adjusted to align the spot array onto the markers, ensuring that the required pitch is obtained.

After all the collimation barrels and Fourier lenses have been adjusted it is possible to align an OPS module in less than 15 min, as follows. When the cells are deposited onto the rods in the baseplate four out of six mechanical degrees of freedom are constrained: Only the roll and the longitudinal position of the elements need to be adjusted. Given that a collimated beam is output from the collimation barrel, the longitudinal alignment of only three elements is critical:

- (1) The FOG must be positioned at the front focal point of the Fourier lens.
- (2) The distance between the Fourier lens and the OPS lenslet array (LA_1) must be equal to the back focal length of the Fourier lens plus f_{LA} such that the output beams of the OPS module are collimated.
- (3) The OPS lenslet array LA_1 must be positioned at a distance of $f_{\text{LA}} \pm 500 \mu\text{m}$ from the PMG after the OPS baseplate is inserted into the interconnect base-

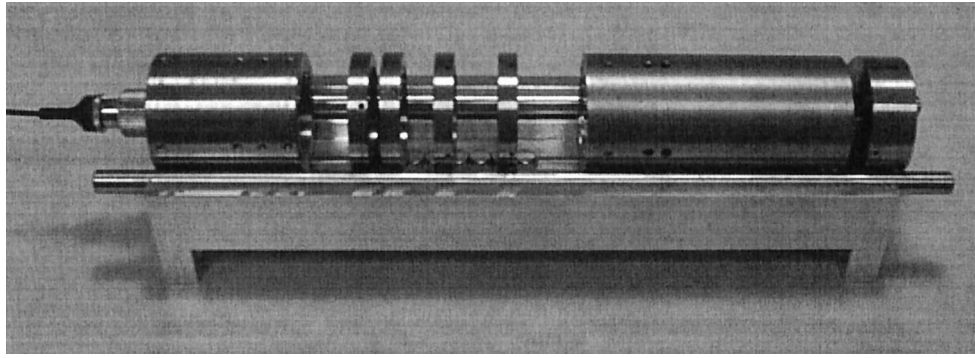


Fig. 9. Photograph of an assembled OPS module.

plate (to preserve the interconnect system telecentricity).

Furthermore, the roll of only three elements needs to be adjusted:

(1) The roll of the FOG must be adjusted so that the spot array at the output of the OPS module is rotationally aligned with the PMG and the interconnect system.

(2) The roll of lenslet array LA_1 must be adjusted so that it is rotationally aligned with the spot array at the output of the Fourier lens.

(3) The roll of the QWP must be adjusted to circularize the light polarization and maximize power transfer to the interconnect system.

The first step in the alignment of an OPS module is to position the Fourier lens by hand to within $200\ \mu\text{m}$ of its ideal position. Next, the position of the FOG is adjusted by the imaging of the grating through the Fourier lens onto a screen placed approximately 50 cm after the Fourier lens. Only when the FOG is at the front focal point of the Fourier lens will a clear image of the grating be visible on the screen. Using this technique allows the position of the FOG to be estimated to be aligned to within $50\ \mu\text{m}$ of the Fourier lens's front focal point. The rotational alignment of the FOG is then performed by rotation of the cell by hand such that the beams at its output are parallel to markers on an alignment mask.

Next, lenslet array LA_1 is deposited onto the baseplate and rotated such that its columns of minilenses are parallel to the incident beams. Because of the imperfect alignment of LA_1 with respect to the mechanical center of its cell, the RPP is then rotated such that each spot of the array is aligned in the center of a minilens. The longitudinal position of LA_1 is next adjusted to collimate the beam by minimization of the divergence angle of the spot array.

Finally, the assembly of the OPS module is completed by the insertion of the QWP into the baseplate and the adjustment of its roll such the power transmission into the interconnect is maximized. This step is performed after the OPS baseplate has been mounted on the interconnect baseplate. A photo-

graph of an assembled OPS module is shown in Fig. 9.

7. Insertion of the Optical-Power-Supply Baseplate into the Interconnect Baseplate

The most critical part of the optomechanical design for the OPS module is its attachment to the interconnect baseplate. To better understand the attachment technique and the packaging of the second stage of the array generator system, we first present a brief overview of the interconnect baseplate. The mounting technique is then described in Subsection 7.B, and the characterization of the insertion repeatability is presented in Subsection 7.C.

A. Overview of the Interconnect Baseplate

The interconnect baseplate is designed as the optomechanical reference to which all modules are aligned (see Fig. 2). For simplicity and ease of assembly the modules are passively aligned by use of rods, holes, and dowel pins. The beam-combination and the beam-relay modules are packaged in the slot of the interconnect baseplate, whereas the OPS and the chip modules are mounted on the baseplate. The technique for the alignment of the PMG (which is part of the beam-combination module) on the interconnect baseplate is shown in Fig. 10. The PMG substrate is precisely diced, and its edges are placed against three dowel pins. A clamp is then used to hold the module in place. The lenslet array in the second stage of the array generator (LA_2) is packaged in the chip module. This chip module is mounted on the interconnect baseplate by the mating of the chip-module holder to two precision-ground dowel pins. This technique is described further in Ref. 22.

B. Optical-Power-Supply Baseplate-Mounting Technique

Each OPS module must be inserted at 90° to the plane that contains the optical axis of the ring interconnect. The attachment of the OPS module to the optical interconnect is achieved by the mating of the rods of the OPS baseplate to holes machined in the interconnect baseplate. The holes have the same specifications as that of the rod-alignment holder (see Subsection 5.A): They are designed to provide a tight sliding-fit clearance for the rods and machined

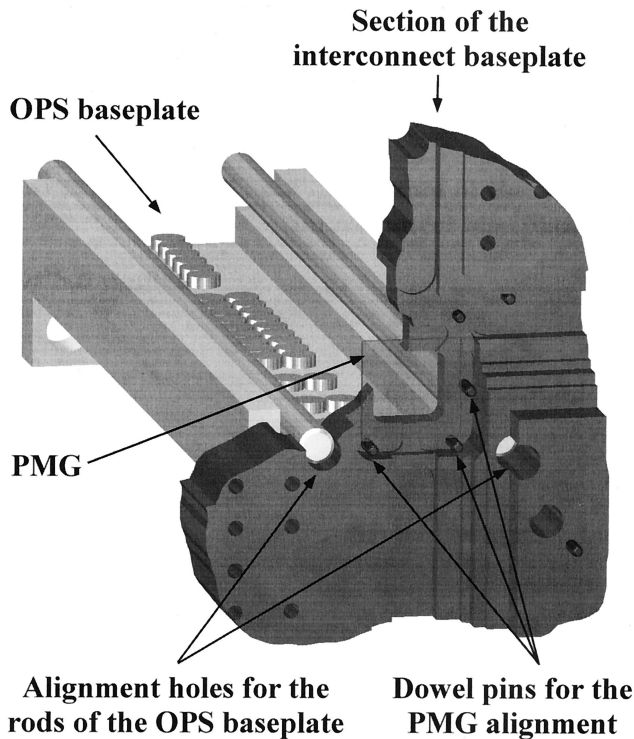


Fig. 10. Schematic diagram of the insertion of the OPS module into the interconnect baseplate.

to within $5 \mu\text{m}$ of the design value. The measured rod diameter is $4.990 \pm 2 \mu\text{m}$, whereas the specification for the diameter of the holes is $5.004^{+0.012}_{-0.000} \mu\text{m}$.

The rods together with the flat surfaces of the baseplates provide a kinematic reference that constrains angular movement (both rotation and tilt). Furthermore, because the optical axis of the OPS module is defined by the two rods, any inaccuracy in the position of the OPS's optical axis is limited to the relative positioning error of the holes in the interconnect baseplate to the other features on the interconnect baseplate. Finally, the OPS baseplate is fixed in place with screws in oversized holes. The mounting of the OPS baseplate to the interconnect baseplate is shown in Fig. 10.

C. Kinematic-Alignment-Mechanism Characterization

To validate the design approach for the mounting of the OPS module, we fabricated a prototypical baseplate. A substrate that replicated the ideal spot array was aligned on the baseplate in place of the PMG and by use of the same technique. The OPS baseplate was removed, reinserted, and secured in place 30 times. For every extraction–insertion cycle, the lateral and the angular misalignments of the beam array with respect to the alignment substrate were noted, and the results are shown in Fig. 11. The average lateral misalignment is $154 \mu\text{m}$ in x and $123 \mu\text{m}$ in y , whereas the average angular misalignment is 0.171° in x and 0.036° in y . The position and the angle of incidence of the beams on the substrate can

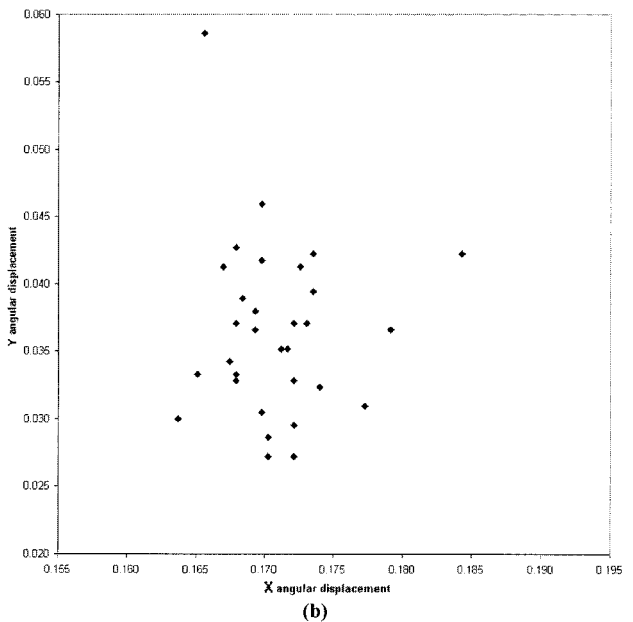
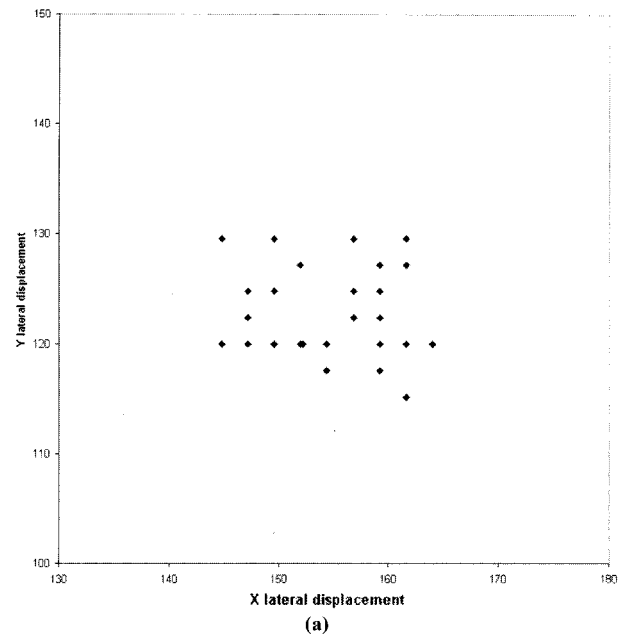


Fig. 11. Characterization of the repeatability of the OPS baseplate insertion: (a) lateral repeatability in micrometers and (b) angular repeatability in degrees.

be adjusted by use of the RPP such that the small misalignments can be eliminated.

The repeatability of the insertion can be characterized by a comparison of the misalignment standard deviations with the alignment tolerance between the OPS module and the optical interconnect for a 1% power loss. These tolerances, which were presented in Table 1, are $55 \mu\text{m}$ (lateral) and 0.05° (angular). The standard deviation for the lateral misalignment is $\sigma_x = 5.8 \mu\text{m}$ and $\sigma_y = 4.1 \mu\text{m}$, whereas it is $\sigma_x = 0.004^\circ$ and $\sigma_y = 0.006^\circ$ for the angular misalignment. The results indicate that, after the RPP has been

Table 3. Characterization Results for the Four OPS Modules

Parameter	OPS 1	OPS 2	OPS 3	OPS 4
Spot pitch (μm)	$1601.2 \pm 0.4 \times 801.2 \pm 0.2$	$1602.0 \pm 0.4 \times 800.7 \pm 0.2$	$1602.2 \pm 0.4 \times 801.5 \pm 0.2$	$1602.4 \pm 0.4 \times 799.7 \pm 0.2$
Fourier lens spot size (μm)	$\omega_x = 13.4 \pm 0.1$ $\omega_y = 13.1 \pm 0.1$	$\omega_x = 13.0 \pm 0.1$ $\omega_y = 12.9 \pm 0.1$	$\omega_x = 13.0 \pm 0.1$ $\omega_y = 12.9 \pm 0.1$	$\omega_x = 13.7 \pm 0.1$ $\omega_y = 13.4 \pm 0.1$
FOG nonuniformity	$12\% \pm 1\%$	$11\% \pm 1\%$	$11\% \pm 1\%$	$11\% \pm 1\%$
PMG nonuniformity	$3\% \pm 1\%$	$4\% \pm 1\%$	$4\% \pm 1\%$	$4\% \pm 1\%$

adjusted to align the beams onto the modulators, the OPS baseplate can be removed and passively reinserted such that all the beams remain aligned on the chip.

8. Characterization

Four OPS modules were implemented, and a detailed characterization of the performance was carried out. The goal was to obtain statistical information on the reproducibility of the design and implementation. The results are presented in the following subsections.

A. Spots and the Spot Array

Three main parameters must be characterized for the spot array: the spot size, the array pitch, and the array power uniformity. The measured values of these parameters for all four OPS modules are shown in Table 3, and a photograph of the spot array at the modulators is shown in Fig. 12. Because the system is telecentric, the spot size at the modulators is the same as that at the output of the Fourier lens. For this reason a beam profiler mounted on a micrometer stage was used to measure the spot size at the back focal point of the Fourier lens. The average value is $13.2 \mu\text{m}$, whereas the worst-case measurement ($13.7 \mu\text{m}$) is within $0.6 \mu\text{m}$ of the design value.

The pitch of the 4×8 array was measured by means of placing a mask at the back focal point of the Fourier lens. The positions of the four outer spots were monitored on the mask, as shown in Fig. 13. The pitch of the array was derived by measurement of the spot displacements from the markers and then distribution of the error over the entire array. This technique allows the evaluation of the worst-case spot pitch because displacements of the outer spots are largest as a result of distortion and aberrations. This also explains the fact that the steeper pitch ($1600 \mu\text{m}$) is not exactly twice as large as the lesser one ($800 \mu\text{m}$). The worst pitch, which is $1602.2 \pm 0.4 \mu\text{m} \times 801.5 \pm 0.2 \mu\text{m}$ (OPS module 3), is within the tolerance of the system. A similar technique was utilized to characterize the spot pitch of the 4×4 array. An OPS module was inserted into the interconnect baseplate, and the pitch of the outermost cluster was measured. The result was $89.1 \pm 0.2 \mu\text{m} \times 89.1 \pm 0.2 \mu\text{m}$, which is excellent.

A common metric for quantifying the uniformity of FOG's is to consider that the power distribution in the array approximates a normal distribution and to calculate the standard deviation. Using this metric showed the measured nonuniformity for the 4×8

array produced by the FOG's to be 12%. However, because the system employs differential encoding and pairs of beams illuminating the modulators and the detectors are created at the PMG, these beams will have the same relative dc offset. Thus the uniformity of the PMG is more critical than that of the FOG. For the 4×4 array generator in the PMG, the average nonuniformity is 4%, and no significant zero-order beam is present in any of the spot arrays. Thus pairs of beams in a data channel will have almost identical power at the modulators.

B. Power Budget and Efficiency

Throughput efficiency measurements were performed on each of the optical elements of the array-generation system, and the averages are listed in Table 4. The values for the diffractive optical elements (FOG, PMG, and lenslet array) include both diffraction and reflection losses. The throughput of all components was within specifications except for the FOG and the PMG. The low efficiency and the high nonuniformity of the FOG are most probably attributable to the difficulty of designing an element that produces such a large diffraction angle. The low efficiency of the PMG is probably attributable to

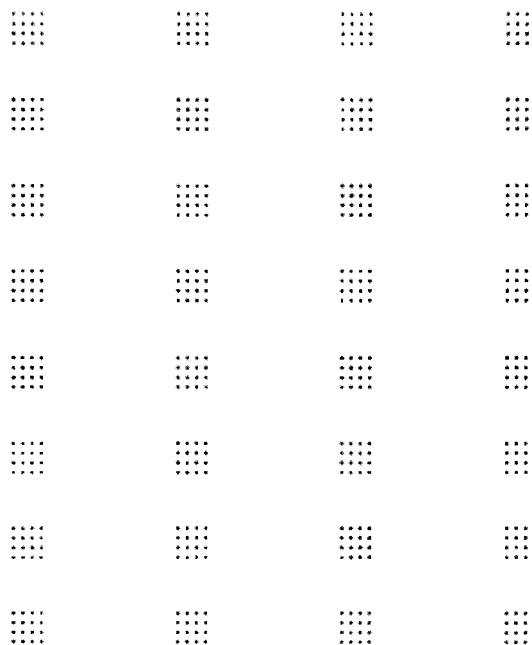


Fig. 12. Photograph of the 512-spot array (the contrast is inverted).

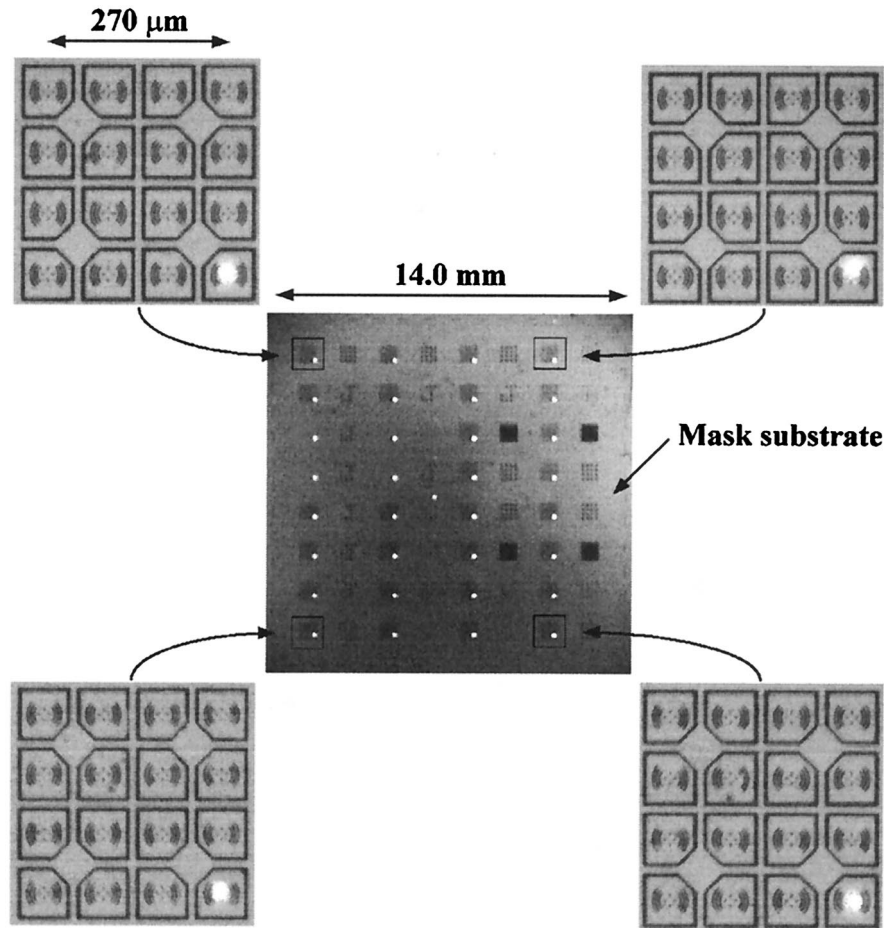


Fig. 13. Photograph of the 4×8 spot array on the mask substrate.

fabrication errors. Given the low efficiency of these two components, the cumulative throughput for the array-generation system was measured to be $33\% \pm 5\%$.

9. Conclusion

A robust, compact, and modular OPS spot-array generator has been implemented successfully to drive an array of 512 modulators used in a free-space optical interconnect. The design requirements presented in Table 1 were met successfully. The optomechanical design for the OPS allows the module to be aligned kinematically to the interconnect system by use of

precision-ground rods and tight sliding-fit holes as a reference. This kinematic alignment results in a module that is both simple to assemble and easy to use. Furthermore, the alignment of the OPS module to the interconnect system is repeatable such that the module can be unmounted and remounted without requiring any realignment. Note that light was routed successfully from the modulators to the detectors in the optical interconnect,²¹ thus further demonstrating that the requirements for the OPS have been satisfied.

This research was supported by the Canadian Institute for Telecommunications Research under the National Centres of Excellence program of Canada, the National Sciences and Engineering Council (NSERC) (grant OG0194547), and the Fonds pour la Formation de Chercheurs et l'Aide à la Recherche (FCAR) (grant NC-1778).

References

1. F. A. P. Tooley, "Challenges in optically interconnecting electronics," *IEEE J. Select. Top. Quantum Electron.* **2**, 3–13 (1996).
2. O. Kibar, D. A. Van Blerkom, C. Fan, and S. C. Esener, "Power minimization and technology comparisons for digital free-space optoelectronic interconnections," *J. Lightwave Technol.* **17**, 546–555 (1999).

Table 4. Throughput Efficiency of the Array-Generation System

Optical Component	Measured Value
Collimation barrel	$99\% \pm 1\%$
RPP	$99\% \pm 1\%$
QWP	$99\% \pm 1\%$
FOG	$70\% \pm 2\%$
Fourier lens	$95\% \pm 1\%$
Lenslet array	$84\% \pm 2\%$
PMG	$72\% \pm 2\%$
Lenslet array	$84\% \pm 2\%$
Total efficiency	$33\% \pm 5\%$

3. C. Fan, D. A. Van Blerkom, W. L. Hendrick, and S. C. Esener, "Free-space optical interconnection: a technology comparison of vertical-cavity surface-emitting lasers and multiple-quantum-well modulators," *Opt. Rev. Jpn.* **3**, 394–396 (1996).
4. A. L. Lentine, "Qualitative comparison of MQW modulator and VCSEL based OE-VLSI: a systems perspective," in *Proceedings of LEOS '97: Tenth Annual Meeting* (Lasers and Electro-Optics Society, Piscataway, N.J., 1997), Vol. 2, pp. 83–84.
5. L. A. Coldren, E. Hegblom, E. Strzelecka, J. Ko, Y. Akulova, and B. Thibeault, "Recent advances and important issues in vertical-cavity lasers," in *Vertical-Cavity Surface-Emitting Lasers*, K. D. Choquette and D. G. Deppe, eds., *Proc. SPIE* **3003**, 2–13 (1997).
6. R. A. Morgan, "Vertical-cavity surface-emitting lasers: present and future," in *Vertical-Cavity Surface-Emitting Lasers*, K. D. Choquette and D. G. Deppe, eds., *Proc. SPIE* **3003**, 14–26 (1997).
7. A. V. Krishnamoorthy, L. M. F. Chirovsky, W. S. Hobson, R. E. Leibengath, S. P. Hui, G. J. Zydzik, K. W. Gossen, J. D. Wynn, B. J. Tseng, J. Lopata, J. A. Walker, J. E. Cunningham, and L. A. D'Asaro, "Vertical-cavity surface-emitting lasers flip-chip bonded to gigabit-per-second CMOS circuits," *IEEE Photon. Technol. Lett.* **11**, 128–130 (1999).
8. A. V. Krishnamoorthy and K. W. Gossen, "Progress in optoelectronic-VLSI smart pixel technology based on GaAs/AlGaAs MQW modulators," *Int. J. Optoelectron.* **11**, 181–198 (1997).
9. D. V. Plant, A. Z. Shang, M. R. Otazo, D. R. Rolston, B. Robertson, and H. S. Hinton, "Design, modeling, and characterization of FET-SEED smart pixel transceiver arrays for optical backplanes," *IEEE J. Quantum Electron.* **32**, 1391–1398 (1996).
10. H. S. Hinton, T. J. Cloonan, F. B. McCormick, A. L. Lentine, and F. A. P. Tooley, "Free-space digital optical systems," *Proc. IEEE* **82**, 1632–1649 (1994).
11. D. T. Neilson, S. M. Prince, D. A. Baillie, and F. A. P. Tooley, "Optical design of a 1024-channel free-space sorting demonstrator," *Appl. Opt.* **36**, 9243–9252 (1997).
12. B. Robertson, "Design of an optical interconnect for photonic backplane applications," *Appl. Opt.* **37**, 2974–2984 (1998).
13. D. R. Rolston, B. Robertson, H. S. Hinton, and D. V. Plant, "Analysis of a microchannel interconnect based on the clustering of smart-pixel-device windows," *Appl. Opt.* **35**, 1220–1233 (1996).
14. N. Streibl, "Beam shaping with optical array generators," *J. Mod. Opt.* **36**, 1559–1573 (1989).
15. H. Dammann and K. Gortler, "High-efficiency in-line multiple imaging by means of multiple phase holograms," *Opt. Commun.* **3**, 312–315 (1971).
16. F. B. McCormick, "Generation of large spot arrays from a single laser beam by multiple imaging with binary phase gratings," *Opt. Eng.* **28**, 299–304 (1989).
17. J. Jahns, M. M. Down, M. E. Prise, N. Streibl, and S. J. Walker, "Dammann gratings for laser beam shaping," *Opt. Eng.* **28**, 1267–1275 (1989).
18. J. M. Miller, M. R. Taghizadeh, J. Turunen, and N. Ross, "Multilevel-grating array generators: fabrication error analysis and experiments," *Appl. Opt.* **32**, 2519–2525 (1993).
19. N. C. Craft and M. E. Prise, "Optical system tolerances for symmetric self-electro-optic-effect devices in optical computers," in *Optical Computing*, Vol. 9 of 1989 OSA Technical Digest Series (Optical Society of America, Washington, D.C., 1989), pp. 334–337.
20. R. Iyer, Y. S. Liu, G. C. Boisset, D. J. Goodwill, M. H. Ayliffe, B. Robertson, W. M. Robertson, D. Kabal, F. Lacroix, and D. V. Plant, "Design, implementation, and characterization of an optical power supply spot-array generator for a four-stage free-space optical backplane," *Appl. Opt.* **36**, 9230–9242 (1997).
21. F. Lacroix, B. Robertson, M. H. Ayliffe, E. Bernier, F. A. P. Tooley, M. Châteauneuf, D. V. Plant, and A. G. Kirk, "Design and implementation of a four-stage clustered free-space optical interconnect," in *Optics in Computing '98*, P. H. Chavel, D. A. Miller, and H. Thienpont, eds., *Proc. SPIE* **3490**, 107–110 (1998).
22. M. H. Ayliffe, D. Kabal, P. Khurana, F. Lacroix, A. G. Kirk, F. A. P. Tooley, and D. V. Plant, "Electrical, thermal, and optomechanical packaging of large 2-D optoelectronic device arrays for free-space optical interconnects," *J. Opt. A: Pure Appl. Opt.* **1**, 267–271 (1999).
23. B. Robertson, Y. Liu, G. C. Boisset, M. R. Taghizadeh, and D. V. Plant, "In situ interferometric alignment systems for the assembly of microchannel relay systems," *Appl. Opt.* **36**, 9253–9260 (1997).
24. A. G. Kirk and T. J. Hall, "Design of computer-generated holograms by simulated annealing: coding density and reconstruction error," *Opt. Commun.* **94**, 491–496 (1992).
25. B. E. A. Saleh and M. C. Teich, *Fundamentals of Photonics* (Wiley, New York, 1991), Chap. 3.
26. W. J. Smith, *Modern Optical Engineering*, 2nd ed. (McGraw-Hill, New York, 1990), Chap. 11.
27. J. L. Brubaker, F. B. McCormick, F. A. P. Tooley, J. M. Sasian, T. J. Cloonan, A. L. Lentine, S. J. Hinterlong, and M. J. Herron, "Optomechanics of a free-space photonic switch: the components," in *Optomechanics and Dimensional Stability*, R. A. Paquin and D. Vukobratovich, eds., *Proc. SPIE* **1533**, 88–96 (1991).
28. F. B. McCormick, F. A. P. Tooley, J. L. Brubaker, J. M. Sasian, T. J. Cloonan, A. L. Lentine, R. L. Morrison, R. J. Crisci, S. L. Walker, S. J. Hinterlong, and M. J. Herron, "Optomechanics of a free-space photonic switch: the system," in *Optomechanics and Dimensional Stability*, R. A. Paquin and D. Vukobratovich, eds., *Proc. SPIE* **1533**, 97–114 (1991).
29. G. C. Boisset, M. H. Ayliffe, B. Robertson, R. Iyer, Y. S. Liu, D. V. Plant, D. J. Goodwill, D. Kabal, and D. Pavlasek, "Optomechanics of a four-stage hybrid-self-electro-optic-device-based free-space optical backplane," *Appl. Opt.* **36**, 7341–7358 (1997).